Title
Assessing High-Throughput Descriptors for Prediction of Transparent Conductors

Journal
Chemistry of Materials, 30(22)

ISSN
0897-4756

Authors
Woods-Robinson, Rachel
Broberg, Danny
Faghaninia, Alireza
et al.

Publication Date
2018-11-27

DOI
10.1021/acs.chemmater.8b03529

Peer reviewed

Assessing High-Throughput Descriptors for Prediction of Transparent Conductors

Rachel Woods-Robinson,[†,‡,¶] Danny Broberg,[§] Alireza Faghaninia,[‡] Anubhav Jain,[‡] Shyam S. Dwaraknath,[‡] and Kristin A. Persson[*,§,‡]

†*Applied Science and Technology, University of California Berkeley, Berkeley, CA 94702*

‡*Lawrence Berkeley National Laboratory, Berkeley, CA 94720, USA*

¶*National Renewable Energy Laboratory, Golden, CO 80401, USA*

§*Department of Materials Science and Engineering, University of California, Berkeley, CA 94720, USA*

E-mail: kpersson@lbl.gov

Abstract

The growth of materials databases has yielded significant quantities of data to mine for new energy materials using high-throughput screening methodologies. One application of interest to energy and optoelectronics is the prediction of new high performing p-type transparent conductors (TCs). However, screening methods for such materials have never been validated over the breadth of computed materials properties. In this study, we compile an experimental data set of 74 bulk crystal structures corresponding to known state-of-the-art n-type and p-type TCs, and compute a series of corresponding computational descriptor properties. Our goals are to (1) compare computational descriptors to experimentally demonstrated properties of real materials in the data set, (2) determine the ability of ground state, density functional theory (DFT)-based computational screening methodologies to identify these experimentally realized TCs, and

(3) use this understanding to estimate reasonable screening cutoffs for four commonly used descriptors. First, stability calculations demonstrate that most materials in the data set have an energy above the convex hull (E_{hull}) of less than 100 meV/atom, and we also propose a Pourbaix analysis technique to estimate moisture stability. Second, we find a lenient cutoff for the DFT PBE band gap of 0.5 eV is sufficient to include a majority of the wide gap candidates and exclude narrow gap compounds. Next, the effective mass, m^*, is found to correlate weakly to conductivity in the p-type materials as compared with n-type materials, which may motivate an increase in the m^* cutoff as well. Lastly, we perform an uncertainty analysis and literature comparison for the branch point energy (BPE), a qualitative descriptor for dopability. We find the BPEs of most n-type materials to lie near the conduction band and those of most p-type materials to lie at mid-gap; this is a significant distinction, suggesting BPE to be a more definitive descriptor for n-type TC materials. By assessing the validity of this simple screening methodology via comparing experimental data to computational descriptors, we aim to motivate and strengthen future materials discovery efforts in the field of transparent conductors and beyond.

Introduction

High-throughput computational screenings are increasingly utilized in rapidly narrowing down a wide material space to identify promising new compounds for energy applications. Since the launch of the Materials Genome Initiative in 2011[1] and the establishment of databases containing electronic structure calculations (e.g. Materials Project,[2] NRELMatDB,[3–5] OQMD,[6] and AFLOWLIB[7]), targeted searches have yielded a plethora of promising material candidates for batteries,[8,9] photoelectrochemical cells,[10–12] and photovoltaics,[13,14] among other applications. A few of these materials have been achieved experimentally, confirming predictions.[15] With the integration of machine learning algorithms, high-throughput synthesis, and high-throughput characterization, the quantity of associated materials data is

growing daily, and thereby so is the capability to shift the materials design paradigm.[16,17] However, in order to accurately screen materials from any of these data sets we need to be certain that we are judiciously choosing our screening ranges based on quantitative correlations between experimental and computational values.

Recently, one such materials screening effort that has garnered momentum is the search for high performance p-type transparent conductors (TCs). While n-type transparent conducting oxides (TCOs) such as Sn:In_2O_3 (ITO),[18,19] F:SnO_2 (FTO),[20,21] and Al:ZnO (AZO)[22,23] have high electron conductivities, high transparency, and prevalence in commercial devices (e.g. solar cell contacts, electrochromic windows, etc.[24]), p-type TCs significantly lag in performance and device integration.[25] Achieving p-type TCs with comparable properties to n-type TCs would enable new solar cell architectures and transparent electronics applications, however finding such materials is still a major challenge.[26] In 1997 Hosono et al. synthesized the p-type delafossite $CuAlO_2$, considered by much of the TC community as the first p-type TCO.[27] For the past two decades, other Cu-based delafossite oxides ($CuMO_2$ with M = Al,[28] B,[29,30] Cr,[31–33] Fe,[34,35] Ga,[35,36] Sc,[37,38] Y[39]) have been explored, as well as spinel oxides (e.g. $ZnCo_2O_4$)[40,41] and layered mixed anion chalcogenides (most notably LaCuOCh[42,43] and BaCuChF.[38] with Ch = S, Se, Te). Unfortunately, the performance of these candidates is still lacking, mostly due to low valence band (VB) dispersion stemming from localized O 2p orbitals, the intrinsic trade-off between conductivity and transparency, and challenges associated with p-type doping of wide-gap semiconductors.

Data mining of computed structures has provided a means to address these fundamental issues and search for wide gap materials with highly disperse valence bands. In 2013, Hautier et al. screened wide-gap oxides in the Materials Project (MP) database for low hole effective masses, resulting in new candidate p-type transparent conductors.[44] A follow-up study proposed a set of promising Bi-based candidates, including a double perovskite Ba_2BiTaO_6. This material has since been synthesized and confirmed p-type with remarkably high mobility, but its conductivity remains low due to low hole concentration.[45] Recently, there has

been a surge of interest in screenings of both oxide and non-oxide materials, in particular phosphides and sulfides which demonstrate potential for higher hole mobilities than oxides.[46] In 2016, a screening of the AFLOWLIB database uncovered new lanthanide-based oxychalcogenide p-type TC candidates X_2SeO_2 (X = La, Pr, Nd, Gd).[47] Subsequently, Varley et al. and Williamson et al. screened for p-type transparent phosphide materials and identified BP and CaCuP, respectively, as particularly promising candidates,[46,48] and other recent studies focused on the prediction of compounds that do not yet exist experimentally.[49] A generic high-throughput screening methodology for p-type TCs from these aforementioned studies, depicted as a screening "funnel" in **Figure 1**, applies relatively inexpensive calculations to an initial set and then sequentially adds more expensive refinements to narrow the final set. Typical screenings use a combination of the following properties and descriptors, arranged roughly in order of low to high computational cost:

- **Stability**: Apply a cutoff to estimate material stability based on chemical potential, formation energy, or competition from other phases to ensure that passing materials are likely synthesizable.[50,51] The energy above the convex hull, E_{hull}, is often used.

- **Transparency**: Screen for transparency to visible light using the descriptor of indirect or direct band gap. Determined from DFT calculations (typical cutoff range used in the literature for screenings is $E_g > 1$–2 eV, e.g. using GGA) or from higher accuracy functionals (e.g. HSE06, GW) for a more accurate but computationally expensive band gap estimate.[52]

- **Mobility and conductivity**: Screen for high predicted hole mobilities (i.e. high conductivity) by calculation of the descriptor of hole effective mass m^* at the upper valence band (typically $m^* < 1$).[53] Note this value is actually normalized by the true electron mass such that $m^* = m^*_{eff}/m_e$; we will henceforth refer simply to the unitless "m^*", or "m^*_e" and "m^*_h" for electron and hole effective masses, respectively. Calculation of scattering time is not yet favorable for use in high-throughput screenings, hence the proxy of effective mass is used.

- **p-type dopability**: Gauge whether a material should be intrinsically p-type dopable or suffers from significant compensation using calculations of various complexity, from bulk structure branch point energies (BPEs)[47,49] to more expensive intrinsic/extrinsic defect calculations.[44,54]

- **Refinements**: Tailor the output set from the preceding calculations to specific areas of interest, e.g. surface slab calculations to estimate band alignment,[52] electrochemical stability, further refinements on optical prop-

erties, materials availability and toxicity considerations, 2D materials calculations to compare bulk structures with monolayers,[54] etc.

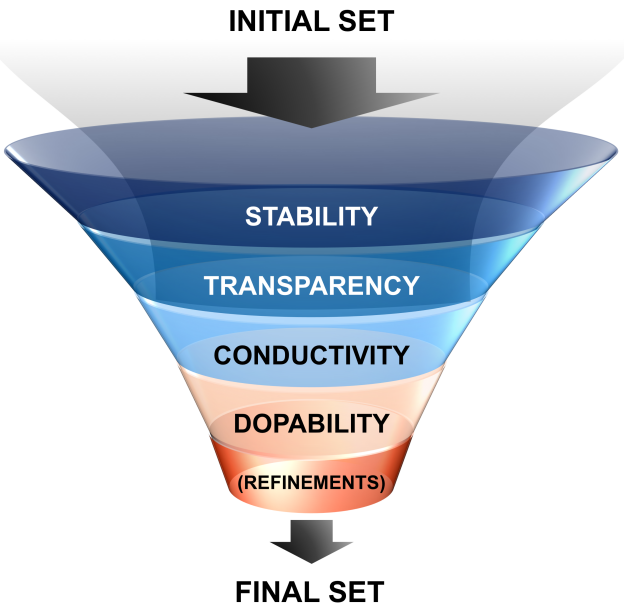

Figure 1: A generic high-throughput computational screening "funnel" for transparent conductors. The first four filters can be derived from density functional theory calculations, and will be explored in this paper. "Refinements" indicate any other screening parameter that might be utilized, such as additional calculations of optical properties or band alignment calculations.

A key approximation employed in many high-throughput studies is that simple, bulk, thermodynamic quantities can serve as proxies for properties of real, engineered materials. However, the effects of surfaces, defects, and alloying in real systems can drastically alter resulting experimentally achievable properties. These non-equilibrium effects are certainly present to a varying degree in known TCs. Here, we will make the assumption that for each chosen bulk, computed thermodynamic quantity X_{thermo} highlighted in this study, non-equilibrium effects can be roughly represented as some perturbation ΔX_{non-eq} such that an experimentally achievable property X_{exp} can be described as:

$$X_{exp} \approx X_{thermo} \pm \Delta X_{non-eq} \tag{1}$$

In anticipation of future screening methodologies and exploration of TCs within continuously growing materials databases, and without *a priori* knowing ΔX_{non-eq}, it is essential

to examine the following: what is a reasonable value and range of calculated ground state descriptors (X_{thermo}) that represent experimental targeted properties of interest (X_{exp})? In previous work aimed at the discovery of new p-type TCs, cutoffs for stability and band gap vary by publication and DFT functional, the hole effective mass limit is typically $m^*_{eff} <$ 1–1.5,[55] and BPE is occasionally used to assess p-type dopability. To our knowledge, no experimentally-based, quantitative justification of selecting any such values in tandem has been reported. In this study, we aim to provide an evaluation of common screening methodologies and assess the appropriate range of the applied screening parameters in broader searches for novel p-type TCs that integrate computational and experimental materials discovery. Specifically, we ask here whether the methodology just described can accurately identify previously synthesized TCs. To accomplish this, we compile a data set of 74 known state-of-the-art n-type and p-type transparent conducting materials, collect and calculate a series of coarse-grain computational descriptor properties from the funnel (E_{hull}, E_g, m^*, BPE) for their corresponding bulk crystal structures, and compare computed values to optimized properties that have been achieved experimentally and commercially. For simplicity, we restrict our analysis to properties requiring only a DFT band structure, corresponding to the first four broad filters of the funnel. By assessing these descriptors for their range of accuracy, we aim to create a benchmarking framework to guide and accelerate future materials discovery efforts.

Methodology

Data compilation and test set

In order to assess the validity of proposed and commonly used screening parameters, we have compiled a comprehensive set of state-of-the-art experimentally achieved n-type and p-type transparent conducting materials from the literature, carefully tabulating the growth conditions, dopants, material type (e.g. polycrystal vs. single crystal), and the space group

corresponding to the undoped crystal structure of each material (c.f. Supporting Information). Selected experimentally tabulated properties include highest measured conductivity and mobility, the range of measured band gaps, the dopings achieved (dopant type and carrier concentration), and the extent to which each material has been explored in the literature as a TC. We explicitly include TCs only with experimentally reported optical band gaps greater than 2 eV, defining those with gaps $E_g \geq 3.1$ eV and conductivities $\sigma \geq 10$ S/cm as "good" and the rest as "ok". This set of experimental studies corresponds to 74 total distinct crystal structures: 29 n-type materials and 45 p-type materials. As shown in **Figure 2**, most of these TCs are oxides, but the p-type set includes more exploratory sulfides such as $CuAlS_2$, mixed anion compounds such as BaCuSeF, and newer, non-chalcogenide compounds such as CaCuP (synthesized only as a pellet). The chosen TC set ranges from commercially viable materials, explored and optimized extensively for over fifty years with a variety of dopants and synthesis methods (e.g. ZnO, In_2O_3, SnO_2), to prospective materials that have been synthesized in only one or two studies so far (e.g. Ba_2BiTaO_6). All experimental values reported are measured at room temperature, and measurement techniques are elaborated upon subsequently when relevant.

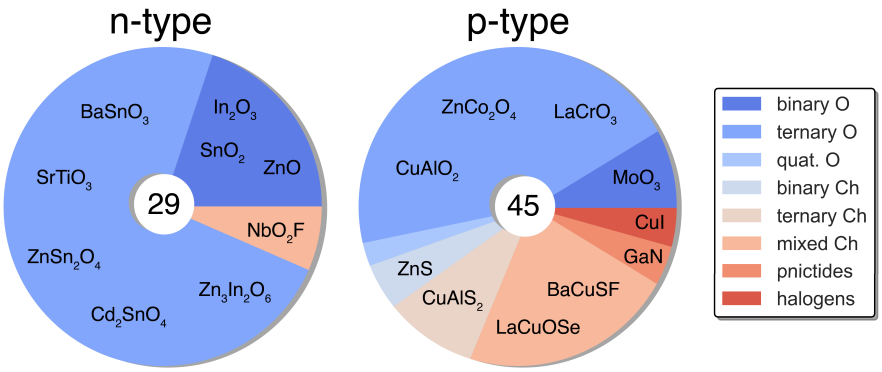

Figure 2: Our transparent conductor test set of 74 materials, designated by material family, with some representative materials denoted (c.f. SI for full list of materials). Although the number of p-type crystal structures is greater than that of n-type structures, any particular n-type crystal structure has been explored in much greater depth than the p-type structures (i.e. number of literature reports, variety of synthesis methods used, number of dopants investigated, number of alloying studies, etc.)

There exist multiple promising pathways to achieving next generation transparent con-

ductors, such as organic TCs (e.g. spiro-OMeTAD),[56] transparent metal nanowire arrays,[57] and the "intrinsic TCs" proposed by Zunger and coworkers.[58] Here, we exclude these material classes and focus solely on "conventional" inorganic, doped, semiconductor TCs because of the large set of experimental candidates to use as a benchmark set. Thus, the screening criteria and associated recommended cutoffs will apply to conventional TCs. Additionally, only single crystal and polycrystalline materials are included in the test set. While amorphous TCs have garnered interest (e.g. n-type In-O-Zn, i.e. IZO)[59] they also incur a significantly higher computational cost and hence, would require an adjusted computational methodology and screening funnel.

We emphasize that the selection and optimization of dopants, strategies of alloying and disordering, and nano-scale engineering (or band engineering) of materials are crucial for achieving high performing transparent conductors. For the scope of this study, however, we focus on computation of undoped, un-alloyed, stoichiometric, ordered materials, i.e. "parent" structures (e.g. ITO is represented by In_2O_3 and Zn:$CuAlS_2$ by $CuAlS_2$) under the assumption from Equation 1 that the properties of these parent structures (X_{thermo}) underlie non-equilibrium properties upon the introduction of dopants and optimization (X_{exp}). Nearly all properties of interest in this paper can be deduced or at least approximated from the DFT relaxed crystal structure and bulk ground state electronic band structure. In summary, the strategy of focusing on bulk, crystalline parent compounds is deliberate, as it is representative of current high-throughput screening methodologies which can be employed with relatively inexpensive computational efforts and thus be efficiently scaled up using workflows that inform more in-depth studies.

Computational methods

Density functional theory (DFT) calculations were extracted from the Materials Project (MP) database for a majority of compounds in the test set.[2] For the 11 compounds not present in databases (c.f. SI), the structures were generated using the structure prediction

algorithm outlined by Hautier et al. according to experimentally reported structure, space group and valence states, and then were relaxed using DFT.[60] These structures have since been incorporated into the MP database. DFT calculations were performed using the projector augmented wave (PAW) method[61,62] as implemented in the Vienna *Ab Initio* Simulation Package (VASP)[63,64] within the Perdew-Burke-Enzerhof (PBE) Generalized Gradient Approximation (GGA) formulation of the exchange-correlation functional,[65] and the Atomate infrastructure.[66] A cut-off for the plane waves of 520 eV is used and a uniform k-point density of approximately 200 per reciprocal atom is employed. In addition, standard MP Hubbard U corrections are used for most transition metal oxides,[67] as documented and implemented in the pymatgen VASP input sets.[68] We note that the computational and convergence parameters were chosen consistently with the settings used in MP to enable direct comparisons with the large set of available MP data.[2] Energy above the convex hull, E_{hull}, is calculated from formation energies relative to their ternary convex hull on MP. The Pourbaix diagrams app on MP is used to calculate the Pourbaix energy above the hull, E_{pb}, using a concentration of 10^{-8} mol/kg.[69] To improve upon PBE band gaps, the HSE06 screened hybrid functional[70] was used to calculate the gaps of the test set and for branch point energy (BPE) calculations (c.f. Equation 4). We also perform a BPE uncertainty analysis.

Effective masses are computed with the Boltzmann Transport Properties (BoltzTraP) code, as employed in previous TC screenings.[71] BoltzTraP is a semi-classical method based on smoothed Fourier interpolation of the bands, which utilizes a temperature-independent and isotropic constant relaxation time approximation (cRTA).[72] Our calculations assume a doping of 10^{20} cm^{-3}, but we include an uncertainty analysis and comparison of density of states effective mass, m^*_{DOS}, in the SI.

Results and discussion

Stability and energy above hull

Thermodynamically stable compounds exhibit an energy above the convex hull, E_{hull}, of 0.0 eV/atom and higher values indicate increasing metastability, though in practice the onset of instability can depend strongly upon kinetics. We can effectively apply the methodology of Equation 1 to assess the degree to which computed thermodynamic stability represents synthesizability. Non-equilibrium synthesis effects can be roughly represented as some perturbation (ΔE_{non-eq}) to the thermodynamic stability (E_{hull}) such that:

$$E_{exp} \approx E_{hull} \pm \Delta E_{non-eq} \tag{2}$$

To be experimentally synthesizable, E_{exp} should be as low as possible. Moisture-sensitivity and degradation through water oxidation in air, which can be prohibitive for synthesis as well as device applications, are estimated using E_{pb}, the Pourbaix stability against decomposition into both dissolved and solid phases.[52,69] We can likewise apply the methodology of Equation 1 to E_{pb}. We note both hull energies are actually free energies of formation of the thermodynamic ground state, ΔG, but refer to them as "E" here for consistency with the literature.

In **Figure 3**, we plot (a) the computed energy above convex hull E_{hull} and (b) the computed Pourbaix stability E_{pb} at neutral conditions ($V = 0$ V, $pH = 7$) for the 74 materials in the test set, both versus the approximate number of experimental literature studies of each material for TC applications (c.f. SI). We note that not only the absolute E_{hull} and E_{pb} are of importance, but also the nature of the predicted decomposition products.[69] Materials that are predicted to decompose to at least one aqueous specie, or through a simple diffusion-less transformation, are kinetically vulnerable. However, for simplicity, here we consider only the absolute thermodynamic metric and observe that stable materials are likely to be found to the left of Figure 3a and Figure 3b, respectively. Specifically, nearly 95% of materials in the

test set have an E_{hull} less than 100 meV/atom, consistent with the findings of Sun et al.[51] Exceptions are the p-type TC materials $CuBO_2$, $ZnIr_2O_4$, CuSCN, and $ZnCo_2O_4$. We note that the two compounds with the highest E_{hull} were generated via our structure prediction algorithm rather than from the ICSD; this could indicate that the relaxed structures (and their bond lengths, bond angles, etc.) are not representative of the experimentally achieved material.

The E_{pb} values of materials in the test set exhibit a wider distribution than the E_{hull} values, with approximately 73% of compounds with an E_{pb} less than 0.5 eV/atom, and $> 90\%$ less than 1.0 eV/atom. This corroborates the findings of Singh et al. that a E_{pb} less than 0.5 eV/atom correlates favorably with stability, 0.5 eV/atom $< E_{pb} <$ 1 eV/atom may passivate, and $E_{pb} > 1$ eV/atom are likely unstable.[52] Exceptions here are the layered mixed anion materials and pnictides; GaN, for example, is predicted to have a high E_{pb}, but has been shown to be stable in water and as a photocatalyst.[73] This discrepancy may be due to the computational underestimation of experimental Pourbaix reference solids for pnictides, namely solid N_2O_5 and P_2O_5, from which we expect an overestimation of Pourbaix instability for nitrides and phosphide compounds. Nevertheless, it is reassuring that in neither case there are materials that lie in the top right section of the graph, signifying that the majority of known, heavily studied TCs fall within previously established ranges of metastability.[51,52]

These two metrics suggest trends, but no definitive synthesizability criteria. We notice no correlation between high E_{hull} and synthesis method; the materials with the highest E_{hull} in Figure 3 have been synthesized with a variety of both physical and chemical deposition methods and at various processing temperatures (c.f. SI). On the other hand, several of these high E_{hull} compounds have been reported to decompose at ambient conditions in the literature including $ZnIn_2O_4$ and $Zn_2In_2O_5$.[74,75] Although some materials may be unstable in their bulk form (e.g. $ZnIn_2O_5$), exploring off-stoichiometries, doping, or alloying with another phase may alter decomposition reaction energies and enhance stability (e.g. alloying $Zn_2In_2O_5$ with $ZnSnO_3$).[76] Additionally, non-equilibrium synthesis mechanisms can stabilize

thermodynamically metastable phases, as shown recently in the space of metastable nitride semiconductors.[77,78] These effects may correlate with a negative ΔE_{non-eq} and effectively reduce E_{exp}. Thus, materials should not be strictly neglected based on this criteria, but Figure 3 reveals that a loose cutoff of approximately $E_{hull} \leq 100$ meV/atom and $E_{pb}(pH{=}7, V{=}0\text{V}) \leq 1$ eV/atom seems reasonable for the screening of bulk materials for TC applications. The exact cutoff is subject to the discretion of the researcher and may vary depending on anion.[50,77]

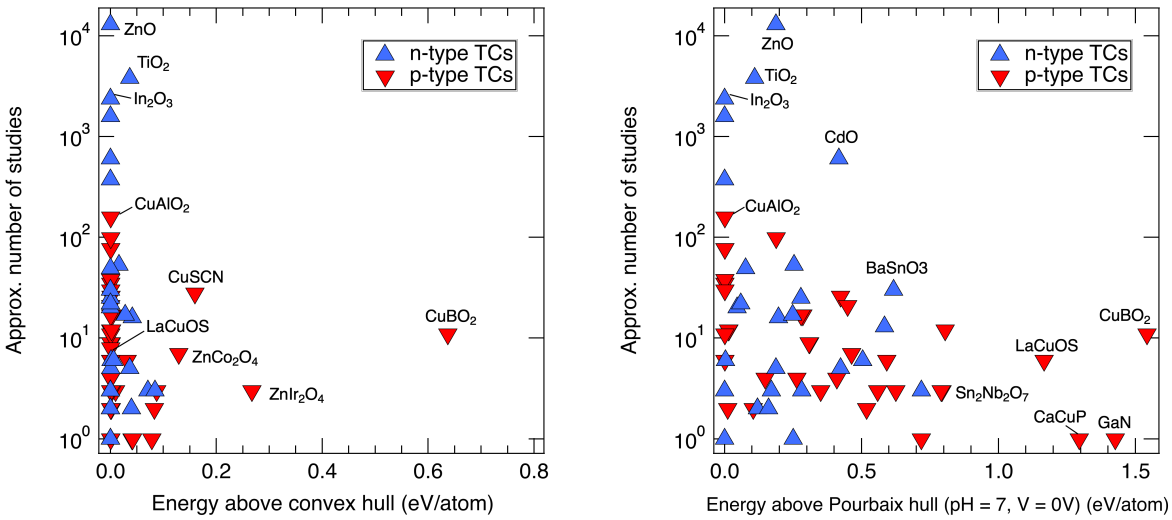

Figure 3: (a) Computed energy above the convex hull E_{hull} and (b) computed energy above the Pourbaix hull, $E_{pb}(pH{=}7, V{=}0\text{V})$, both plotted as a function of number of experimental reports in the literature.

Transparency and DFT band gap

High transparency in TCs is the result of limited absorption in the visible spectrum, typically within 380−750 nm. In semiconductors, absorption in the visible regime occurs primarily due to fundamental band-to-band (interband) transitions, so the base requirement for transparency is a wide optical band gap ($E_g \geq 3.1$ eV, typically). Additionally, optical transparency in TCs is limited by absorption from defect levels, free carrier absorption at high dopings, and excitonic absorption (usually in highly crystalline materials and at low temperatures),[79] but screening for these parameters is more complicated and has not yet

been incorporated into high-throughput studies. As a first-order descriptor of transparency, high-throughput screenings of TCs conventionally focus on band gap calculations, sometimes screening first with a relatively inexpensive functional (e.g. PBE) and then, for a fewer number of candidates, applying more time-consuming calculations using e.g. HSE06 functionals or the GW approach. It is also of increasing interest to screen based on computed direct band gaps, since absorption between indirect gaps involving significant phonon-assistance can be low in some materials, causing direct band-to-band transitions to dominate absorption.[46] Additionally, degenerate doping, microstructure, and phase impurities in real materials can significantly alter the absorption profile. Hence, in the following analysis, bulk measurements and calculations are not directly compared. Instead, we wish to ascertain whether the computed, thermodynamic ground state band gap provides an appropriate descriptor for whether a material selected from screening may be optically transparent upon optimization (c.f. Equation 1), and if so what a reasonable cutoff range could be.

In **Figure 4** we plot the computed gaps of both (a) PBE GGA (or PBE GGA+U for transition metal compounds) and (b) HSE06 functionals for the TC bulk structure test set as a function of the experimentally achieved band gap. For indirect gap semiconductors, which constitute approximately 40% of the test set according to PBE and HSE06 calculations, we choose to plot indirect computed gaps because the experimentally reported values we have tabulated are indirect. The experimental studies included are for both undoped and doped compounds, and for various material quality (thin films, single crystals, pellets). Experimental gaps are plotted as bars to indicate the range of band gap by study, dopant, and processing conditions (c.f. data in SI), hence square data points indicate a singular value reported in the literature. For consistency with the rest of this study, we only review publications of materials explicitly synthesized for TC applications. The experimental gaps reported here have been estimated for thin films with UV–Vis absorption spectrophotometry using Tauc analysis[80] and in bulk samples using diffuse reflectance measurements.[81] We also plot experimental gaps as a function of direct computational PBE and HSE06 gaps in the

SI, and find similar trends (c.f. SI).

Across the test set, PBE consistently underestimates band gap; PBE gaps are approximately 1.3 eV lower on average compared to HSE06 gaps (c.f. SI for PBE versus HSE06 comparison).[82] This is not surprising, as PBE is known to systematically underestimate band gap by 50−100%.[83] However, interestingly, Figure 4 indicates that a conservative cutoff PBE gap of 1 eV excludes approximately half of the state-of-the-art TCs, many of which have achieved experimental gaps ≥3.1 eV (i.e. "transparent"). Thus, we would expect that a cutoff of 1−2 eV would correlate with transparency due to typical PBE underestimates. Instead, we find that lowering the cutoff to 0.5 eV includes >87% of the TCs in this set. This justifies a PBE gap screening cutoff of 0.5 eV, which seems a reasonable GGA cutoff because it screens out highly absorbing compounds, as shown in the SI for a set of Cu chalcopyrite materials. HSE06 gap cutoffs could also be reduced to approximately 2.0 eV with a similar degree of selectivity, however we acknowledge that for practical purposes it may be sensible to retain a higher cutoff to increase selectivity.

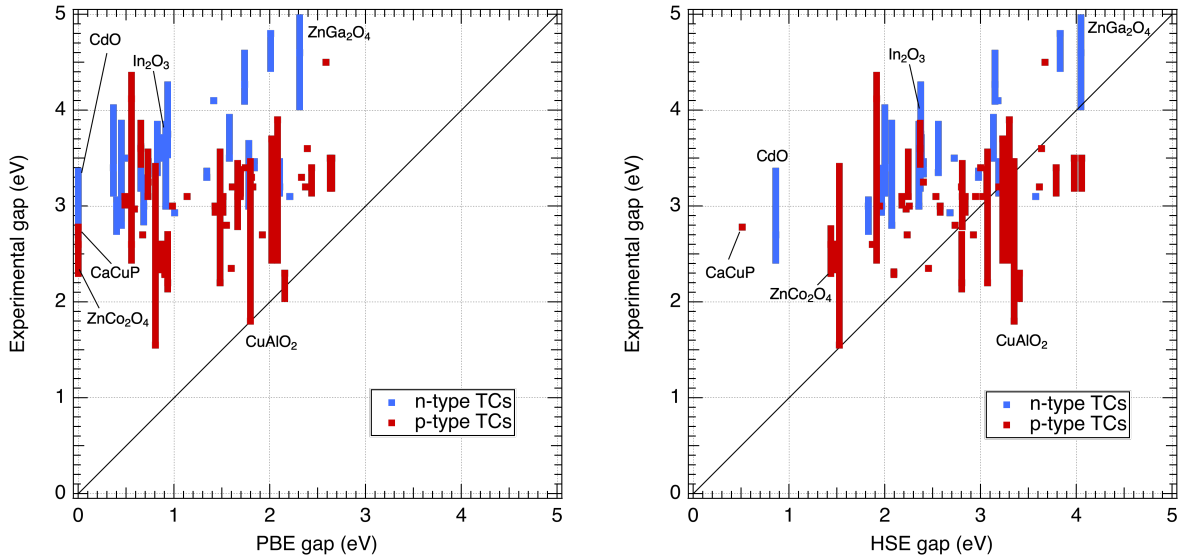

Figure 4: The range of experimental band gap of n-type and p-type transparent conductors in the literature due to various dopants and processing conditions, plotted as a function of (a) indirect PBE GGA band gap and (b) indirect HSE06 band gap. Representative candidates are labeled. Square data points indicate only one value found in the literature, and bars indicate a range. Base materials are those included in the test set.

We also observe a systematic underestimation of the band gap by HSE06 as compared to the experimentally achieved gaps in these TCs. We note that this is not prevalent in the literature across all chemical systems and structure; Yan et al., for example, observed the opposite trend in a large survey of Mn- and V-based oxides.[84] Both the experimental measurements and HSE06 calculations contain significant uncertainties which could influence discrepancies in Figure 4. Tauc band gap analysis, in which the quantity $(\alpha h\nu)^{1/r}$ is plotted versus photon energy $h\nu$ to determine the absorption edge, requires knowledge of whether a gap is direct ($r = 1/2$ for allowed, $r = 3/2$ for forbidden) or indirect ($r = 2$ for allowed, $r = 3$ for forbidden). This information is not always known *a priori* and can lead to errors in reported band gap, e.g. up to ± 0.5 eV in $CuCrO_2$.[85] Additionally, the sharpest absorption edge is typically defined as the gap, but due to tail states (from defects, non-idealities, and low probability transitions in the crystal) defining an exact onset can be somewhat arbitrary.[86] Due to symmetry considerations, in some materials optical transitions at the band edges are forbidden such that the optical gap is significantly wider than calculated electronic gap (e.g. postulated in ITO, FTO and spinel n-type TCOs).[87]

On average for a given computed gap, the n-type TCs represented in this set systematically exhibit marginally larger experimental gaps than the p-type TCs. This can be explained in part by the Burstein-Moss (BM) shift, ΔE_g^{BM}.[88,89] In heavily doped n-type semiconductors, the lower valley of the conduction band (CB) becomes filled with free electrons. In certain TCs without significant mid-gap defect levels, absorption occurs between the valence band maximum (VBM) and the Fermi level above the conduction band minimum (CBM). This causes the optical band gap E_g to increase from the fundamental gap E_g^0 with higher doping such that $E_g = E_g^0 + \Delta E_g^{BM}$. To our knowledge, a BM shift has not been observed in any of the p-type TCs in this set. Rather, addition of dopants in p-type TCs tend to cause the absorption onset to shrink due to mid-gap defect levels, inducing a trade-off between transparency and conductivity.

The BM effect is an example of how descriptor properties are interconnected and, in

the case of TCs, can positively influence one another. There are three main factors that determine and limit ΔE_g^{BM}. Specifically, (1) small effective mass m^* and (2) large dopant levels n (which are target properties of TCs) increase ΔE_g^{BM}, corroborating its presence in n-type TCs but not p-type TCs:

$$\Delta E_g^{BM} = \frac{h^2 n^{2/3}}{8\pi^{2/3} m^*} \tag{3}$$

However, this equation assumes a single, parabolic band configuration, which indicates the magnitude and intrinsic limits of the BM shift depend on (3) the shape and spacing between bands. Since n-type TCs typically exhibit single-valley and degenerate CBMs, this shift can reach up to 0.5 eV in ITO and Ga-doped ZnO.[90,91] In contrast, most p-type TCs exhibit multiple, shallow valence bands (VBs), not a single-valley VBM. These three factors compound in the test set's p-type TCs such that no noticeable ΔE_g^{BM} occurs. However, this does not rule out the possibility of a BM shift in future p-type TCs, as long as the electronic band structure is composed of a relatively disperse single VB.

We reiterate that a wide gap does not necessarily guarantee transparency. This shift of Fermi level at higher dopings can also present a second fundamental limitation to transparency that is significant to TCs. With high dopings, intraband transitions will start to occur in the infrared, and as doping is increased this can cause absorption in the visible spectrum. This induces a long wavelength transparency cutoff for TCs, and is another reason that an intrinsic trade-off exists between transparency and conductivity.[92] In the SI we use the simple Drude model and computed dielectric tensors to estimate that free carrier absorption in the test set approaches the visible regime for doping levels between 10^{21} and 10^{22} cm^{-3}, depending on material.[26] This onset could induce significant absorption tails in the long wavelength visible regime in highly doped materials, and is likely more detrimental in materials with lower effective masses and smaller dielectric responses (c.f. SI). In direct contrast to the BM effect, in this case a low m^* and doping reduces optical transparency. We note that this simplified model does not incorporate effects stemming from a particular

crystal lattice, and has been shown to be inaccurate in practice.[93] Excitonic absorption has proven to be significant in certain TCs, e.g. in epitaxially grown LaCuOS near the band gap,[94] but screening for these transitions is beyond the scope of this investigation. Additionally, we have found that nearly all "conventional" TCs fall within the range where the HSE06 computed indirect gap is similar to the computed direct gap (c.f. SI), with the exception of several of the p-type oxide delafossites (whereof many exhibit poor transparency), MoO_x, and CaCuP. However, this result does not necessarily limit future design parameters; new potential TCs could have weak indirect transitions and be otherwise transparent. Screening for p-type TCs with wide direct gaps is indeed a promising direction, as demonstrated by Varley et al. among others.[46]

In summary, we have shown that experimentally reported band gaps tend to be larger than computed gaps, to a greater degree than expected by known DFT underestimation consensus, though the differences are systematically greater in n-type than p-type materials. Screening the test set of known TCs using a liberal PBE band gap cutoff of 0.5 eV yields >87% of the initial set; screening with a HSE06 band gap cutoff of 2 eV yields a similar output. However, researchers still need to be aware that reducing the cutoff may increase the risk of including more false positives.

Conductivity and effective mass

Achieving high conductivity in a transparent semiconductor is contingent upon (1) a high effective mass (m^*), (2) reduced internal scattering mechanisms, and (3) sufficient doping to achieve a reasonable concentration of charge carriers (electrons or holes). The first two factors determine mobility (μ), which is routinely calculated by a variety of methods ranging from ab-initio to empirical, as reviewed in the SI. The main distinctions are the degree to which different carrier scattering mechanisms (i.e. carrier relaxation time, τ) are incorporated, and the method of interpolating band structure to estimate m^*. In degenerately doped TCs (e.g. most n-type, and highly conductive p-type such as LaCuOSe[43]) where carrier concentration

ranges from 10^{19} to 10^{21} cm^{-3}, ionized impurity scattering dominates and mobility is approximately temperature independent.[26] Previous TC screenings have employed either the BoltzTraP m^* or parabolic density of states effective mass m^*_{DOS} as the transport descriptor. In this work we use the BoltzTraP code with the constant relaxation time approximation.[71] For comparison, we compile m^*_{DOS} from the NREL materials database in the SI and note the values are significantly higher than BoltzTraP m^*.[3–5]

The ideal benchmark would be comparing computed mobility to experimental mobility. However, computing mobility requires the determination of τ, which is non-trivial to calculate and can vary by orders of magnitude depending on structure, grain size, synthesis conditions, etc. Thus, using m^* as a computational screening descriptor provides a property which is independent of the scattering mechanism. Furthermore, experimental mobilities are typically determined by measuring the Hall effect in a van der Pauw contact configuration,[95] but the accuracy of conventional table-top DC Hall mobilities (room temperature, with < 2 Tesla magnets) below 1 cm^2/Vs exhibits limited accuracy.[96] Experimental mobilities above 1 cm^2/Vs or more accurate AC hall mobilities are reported for less than half of the compounds in our experimental test set (c.f. SI for discussion of experimental mobility). We prefer an experimental metric that (1) represents heavily studied, high performing materials, (2) also represents lower performing prospective materials, and (3) is reported consistently and credibly in the literature. By using the experimental conductivity as a descriptor, we satisfy all three requirements, with the disadvantage of compounding the effects of mobility and carrier concentration.

Figure 5 shows the highest reported experimental values of conductivity across the state-of-the-art TCs versus the average BoltzTraP effective mass (m^*_e for n-type and m^*_h for p-type) on a log-log scale. The data points are scaled in size, according to the number of literature reports that investigate each material as a TC, to give a sense of the degree of optimization of each material (c.f. Figure 3 and SI). m^* is calculated assuming a carrier concentration of 10^{20} cm^{-3}, since this best represents the range of carrier concentrations in

practical transparent conductors.[26] We evaluate m^* at other carrier concentrations to set computational error bars to ±0.09 (c.f. SI for sensitivity analysis). For Figure 5 we average m^* in the x, y, and z directions, since most TCs are polycrystalline and conduct isotropically. An exception is highly non-isotropic and epitaxially grown layered materials (e.g. LaCuOSe), for which we plot m^* in the planar (x-y) direction only (c.f. SI) and notate with diamond-shaped markers. We comment that ambipolar TCs ZnO, SnO_2, and $SrTiO_3$ appear twice in Figure 5 because they are present in the test set as both n-type and p-type TCs. For example, ZnO is intrinsically n-type and can be doped to high electron conductivities by e.g. Al. However, high p-type doping by e.g. N has proven more difficult due to a compensation reaction.

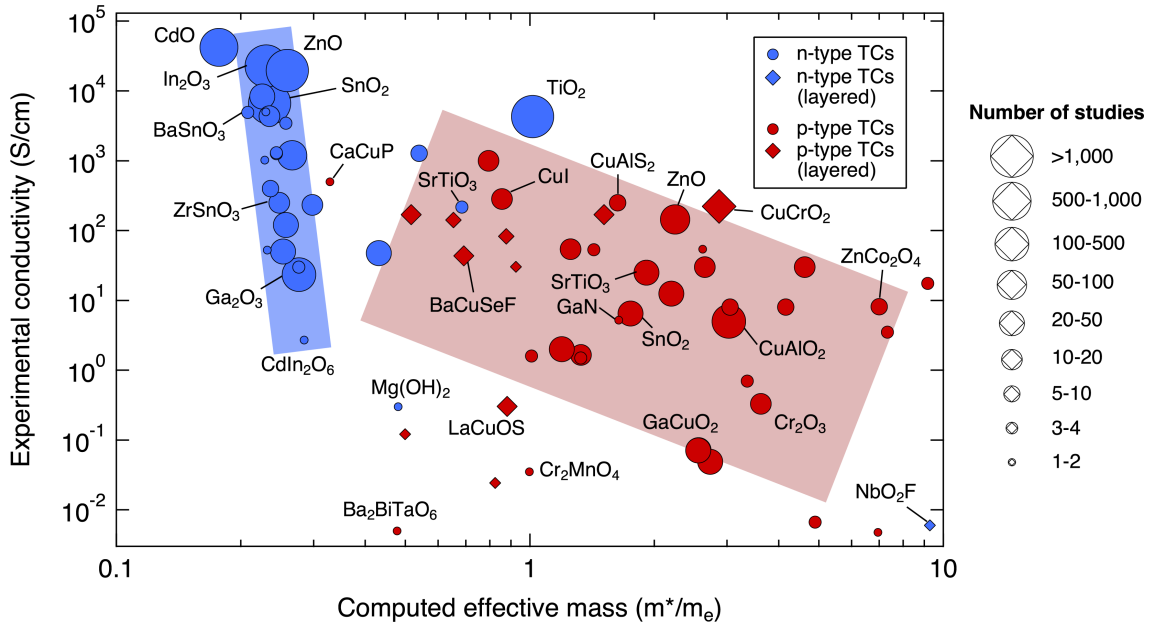

Figure 5: Highest reported values of conductivity of crystalline or polycrystalline state-of-the-art transparent conductors in the test set plotted as a function of computed average effective mass (m_e^* for n-type, m_h^* for p-type, m^* in general). m^* is computed from the BoltzTraP method at $n = 10^{20}$ cm^{-3} and $T = 300$ K, using PBE GGA (or GGA+U for transition metals) relaxed band structures, and is normalized by the electron rest mass m_e such that m^* is unitless. n-type TCs (blue) and p-type TCs (red) are both plotted as circles scaled according to the number of studies published on the particular material (with different dopants, processing conditions, etc.). Some of the most prominent TCs and a few outliers are labeled. For layered, epitaxially grown, c-axis oriented materials (squares), m^* is averaged over the planar direction (x-y plane) rather than isotropically. These m^* values may be underestimated due to non-idealities in the crystal. Red and blue boxes are guides to the eye, not a fit. Error bars of computed m^* are approximately ±0.09, as determined by calculations at various carrier concentrations (c.f. SI, as well as for discussion of outliers).

The experimental conductivity in both n-type and p-type TCs appears to correlate in-

versely with computed m^*, as expected from band theory. However, there is a stark contrast in distribution, slope, and magnitude between the n-type TC set and the p-type TC set. Colored boxes designate an effective range that most of these materials lie within. n-type TCs (blue box) have a sharp slope, a narrow distribution, and are clustered in the top left of the plot, with most m_e^* less than 0.4 and conductivities up to the order of 10^4 S/cm. The four TCs used most prominently in commercial applications – ZnO, In_2O_3, SnO_2, and CdO – are located farthest to the top. This strong correlation is likely due to the fact that nearly all these n-type TCs are oxides with a single valley, metal s-character conduction band. The m_e^* is relatively comparable (approximately $0.2-0.3$) over a wide range of conductivities; it has been suggested that conductivity within s-band n-type conductors may depend more on cation octahedral site density than on m_e^*.[97] TiO_2 is a noticeable outlier in the set; this may arise from its $3d$-character conduction band, which possesses more localized (flat) dispersion.[98] n-type NbO_2F is another exception, with a very low m_e^* and high mobility; it is also not an s-band conductor.[99] p-type TCs also seem to follow an inverse proportionality (red box), but m_h^* and conductivity appear less correlated across the set than in the n-type TCs. Additionally, many materials are clustered in the bottom of the figure, with low m_h^* but low conductivity. We observe that in p-type TCs where carrier concentration is reported (approximately half of this set), all materials with conductivities less than 5 S/cm have carrier concentrations less than or equal to 10^{18} cm^{-3}. For example, Ba_2BiTaO_6 and $CuGaO_2$ have reported carrier concentrations of approximately 10^{15} cm^{-3} (c.f. SI). This is indicative that many of these materials are limited by their poor dopability. Unlike n-type TCs at the CBM, these p-type TCs possess a variety of VBM orbital hybridization schemes, as well as nearby bands contributing to dispersion, which helps explain their wider distribution.

It is not surprising that the m_e^* in n-type TCs are much lower in magnitude than m_h^* in p-type TCs. Hautier et al. showed that, within available materials databases, intrinsic limitations to achieving highly dispersive valence bands result in a much lower number of low m_e^* oxides as compared to low m_h^*.[44] In wide-gap metal oxides, which comprise most materials in

the set, the upper VB states are dominated by the O $2p$ character which is far more localized than the metallic s orbitals at the bottom of the CB in n-type TCs. This VB dispersion has been shown to increase upon hybridization with metallic $3d$, but it still remains low. To our knowledge, the extent to which this limitation influences the experimentally achievable conductivities of state-of-the-art TCs has not been comprehensively investigated. Figure 5 demonstrates that very few high performance p-type TCs from the literature actually have $m_h^* < 1$, with the exception of the layered structures with low m_h^* in the planar direction. We cannot simply extrapolate the m_h^* vs. conductivity trend in p-type materials to lower m_h^* values. It remains to be seen if a low m_h^* TC that permits high hole doping can be developed and, if so, whether its conductivity could indeed reach the magnitude of state-of-the-art n-type TCs.

Despite higher m_h^*, p-type TCs have reported conductivities up to 10^3 S/cm. n-type TCs, on the other hand, have only achieved conductivities this high in materials with m_e^* of 0.2–0.3, with the exception of TiO_2. This could be due to a variety of reasons. First, discrepancies in optical properties in our two TC sets may contribute to their varied distribution in Figure 5. Experimental band gaps in the test set of n-type TCs are nearly all >3.1 eV, and have similar s-band transitions. Reported p-type candidates, however, are experimentally far more absorbing; several of them exhibit metallic conductivity, with reported transparencies only 30-50% in the visible (e.g. $CuAlO_2$). As shown in Figure 4, p-type TCs in this set have an experimental band gap 0.7 eV smaller than n-type TCs, on average. Since smaller gaps tend to correlate with higher conductivity due to shallower defects and higher dopability, it is reasonable that the p-type candidates here have achieved higher conductivities than n-type at a given m^* due to their somewhat stronger absorption.

Second, the extent of experimental investigation and optimization differs substantially for each material. Many of the n-type TCs in the test set have been studied extensively, and optimized with a variety of dopant and growth conditions to enhance conductivity and mobility. For example, the TC literature for n-type ZnO consists of over 1,000 experiments

using at least 16 different dopant elements and a broad variety of chemical and physical synthesis routes (the result we plot comes from Ga:ZnO grown epitaxially with PLD);[100] its properties have been significantly improved over the past fifty years, and its resistivity is close to the theoretical limit.[101] As indicated by the magnitude of data points in Figure 5, p-type materials have been far less heavily optimized. It is likely that with more synthetic efforts and exploration of dopants, performance could be enhanced to approach theoretical limits. Additionally, Figure 5 reports the *best* results achieved in the lab (mostly epitaxial films or single crystals for n-type TCs, and only a few epitaxial films for p-type TCs) after years of optimization, rather than the typical values of polycrystalline films used in practical applications. Polycrystalline TC samples are likely partially limited by grain boundary scattering which, if eliminated, could lead to higher conductivities.[102] Several of the p-type materials in Figure 5 are polycrystalline, which could help explain the spread.

To summarize this section, we return to the observation that for a particular computed effective mass, conductivities of p-type TCs range over orders of magnitude depending on material. As an example, Figure 5 shows that for $m_h^* \approx 1$, the highest achieved p-type conductivities range from <0.1 S/cm in Li:Cr_2MnO_4[103] to >280 S/cm in off-stoichiometry CuI.[104] This is in part due to different transport mechanisms, and thus wildly different values of scattering time τ (c.f. SI). In Li:Cr_2MnO_4, carriers are thermally activated near room temperature and experience variable range hopping at low temperatures, while CuI exhibits degenerate hole conductivity at room temperature and its temperature dependence can be fit using the fluctuation-induced tunneling conductivity model.[104] Wide gap oxides such as Cr_2MnO_4 also have a tendency for polaronic transport, which can significantly limit mobility.[105] Again, simply having a low m^* does not guarantee high conductivity. A material must be amenable to doping or alloying to achieve adequate carrier concentrations. CuI has a hole concentration almost 10^{20} cm^{-3}. Though Li was calculated to be highly soluble in Cr_2MnO_4, it remains to be shown whether it is indeed an optimal dopant (carrier concentration is not reported),[103] and it could be limited by dopability as is the case for Ba_2BiTaO_6.

This discrepancy could also be due to factors previously discussed; for example Cr_2MnO_4 has only been examined once as a TC, while CuI has been extensively studied. Although effective mass does not tell the full story, by comparing the computed effective masses with the highest experimentally achieved conductivities we have provided insight into the different physical transport mechanisms governing n-type and p-type TCs. This understanding motivates more inclusive screening cutoffs in computational searches for p-type TCs.

Defects and dopability

As described in the previous section, in addition to high intrinsic carrier mobilities, elevated conductivity in TCs requires that a semiconductor is sufficiently n- or p-dopable such that carriers are mobile and compensation is limited. This is a more nuanced requirement than our previous descriptors, and is far more difficult to ascertain in a high-throughput manner. Dopability and selection of adequate dopants requires (1) sufficient solubility of dopants, (2) tolerance of bulk structure to off-stoichiometries, (3) shallow defects that can be thermally activated, and (4) negligible "killer defects", among other factors.[106] Additionally, the presence of defects in a crystal can change absorption properties, which may induce decreased transparency for a system with mid-gap defects.

Several screenings for TCs and other materials have computed the branch point energy (BPE), also known as the charge neutrality level, as a rough assessment of a material's inherent n-type and p-type character.[47,49,107] The BPE averages the CB and VB dispersion to provide an estimate of the intrinsic Fermi level using only the bulk DFT band structure:

$$BPE = \frac{1}{2N_k} \sum_k \left[\frac{1}{N_{VB}} \sum_i^{N_{VB}} \epsilon_{ik} + \frac{1}{N_{CB}} \sum_i^{N_{CB}} \epsilon_{ik} \right] \tag{4}$$

where N_k is the number of k-points sampled in the Brillouin zone, N_{VB} and N_{CB} the number of bands averaged over in the VB and CB, respectively, and ϵ_{ik} the energy eigenvalues at each k-point, respectively (usually a weighted average). Thus, a BPE close to or in the

CB suggests that donor defects are shallow and n-type dopability is more favorable, and a BPE close to or in the VB suggests that acceptor defects are shallow and p-type dopability is more favorable. A BPE in the middle of the gap indicates there is not enough information to determine dopability, and the material might be n-dopable, p-dopable, ambipolar, or negligibly dopable. We note BPE will also vary depending on the DFT functional used, the number of k-points in the DFT calculation, the number of bands included in averaging (as well as the dispersion and proximity of such bands), and whether the averaging occurs over high symmetry lines or over all k-points. The selection and symmetry dependence of N_{CB} and N_{VB} has been validated in the literature for binary zincblende structures,[107] though to our knowledge no consensus on optimal values has been arrived at for other crystal structures.[108]

Here, we calculate BPE for the TC test set to assess its ability to predict whether a TC material is n-type, p-type, or ambipolar dopable. Resulting band alignment to BPE is plotted in **Figure 6**, aligned to the dotted line where $N_{VB} = 4$ and $N_{CB} = 2$ (notated as N_{VB}:N_{CB} = 4:2). We calculate BPEs using HSE06 band structures, following the procedure outlined in Schleife et al.[107] Since the value of BPE depends significantly on the N_{VB} and N_{CB} included in the weighting scheme, and since there is not yet a consensus on which weighting scheme to use, we calculate BPE for seven different configurations (N_{VB}:N_{CB} = 1:1, 2:1, 2:2, 2:4, 4:2, 6:3, 8:4) and indicate the range of computed values with the error bars in Figure 6 (c.f. SI for uncertainty analysis to motivate this selection). We note that the error bars span the range of BPE values computed for all seven configurations, which is why they are not centered around the dotted line. Most of these configurations consider more VBs than CBs; we explicitly exclude band configurations with $N_{VB} \ll N_{CB}$ in defining the error bars because systematically this leads to a BPE in the CB for almost all systems; thus these weights do not contribute to any physical understanding. This approach gives a higher degree of confidence in BPE values compared to selecting only one N_{VB}:N_{CB} configuration. We used full Brillouin zone symmetry but did not consider band crossings in these calculations, since it is not standard to do so in high-throughput studies.

We emphasize that the classification and coloration of materials in Figure 6 are the result of an exhaustive literature review, not based on the BPE calculations presented here. Materials with literature reports of only n-type or only p-type dopability are labeled "only n-type dopable" (blue, far left) or "only p-type dopable" (red, far right), and retain the same classification throughout the text. Those with both n-type and p-type reports are labeled "ambipolar"; we further classify as "ambipolar, intrinsic n-type" (light blue) if the undoped, stoichiometric material has been reported in the literature as n-type doped, and likewise for "ambipolar, intrinsic" (light red). To clarify, some of these labels divide materials into different categories than previously presented in this study. Specifically, in Figures 2-5, we label materials "n" or "p" based on whether they have been explicitly studied as n-type or p-type TCs (c.f. SI). In Figure 6, in contrast, the materials labeled "ambipolar, intrinsic n-type)" are those that have been shown to be intrinsically n-type doped in the literature (considering *all* literature studies, not just TC studies), yet p-type dopable with incorporation of an extrinsic dopant. For example, $SrTiO_3$ has been explicitly studied both as an n-type TC (e.g. La-doped)[109] and a p-type TC (e.g. In-doped).[110] Thus in Figures 2−5 it appeared in both the n- and p-type set. Since it has been shown experimentally to be intrinsically n-type, in appears in the "ambipolar, intrinsic n-type" category in Figure 6. However, even though ZnS has been shown to be intrinsically n-type (undoped), it has only been studied as a p-type TC; thus, in Figures 2-5 it is categorized as a "p-type TC", whereas in Figure 6 it is denoted "ambipolar, intrinsic n-type".

We observe distinct BPE trends in n-type and p-type dopable materials. Almost all of the n-type TCs have a BPE in or near the CB, within the bounds of uncertainty due to band averaging schemes. Specifically, $> 85\%$ of n-type materials have a BPE that lies in or above the upper quartile of the band gap. For example, CdO has its BPE deep in the CB, which corroborates literature values,[107] while $SrSnO_3$ has a BPE $0-0.5$ eV below the CB. This is suggestive that donor defects are shallow and that n-type doping is most probable. Outliers in this set are NbO_2F and $Ca_{12}Al_{14}O_{33}$. NbO_2F has a nearly flat CB and only very

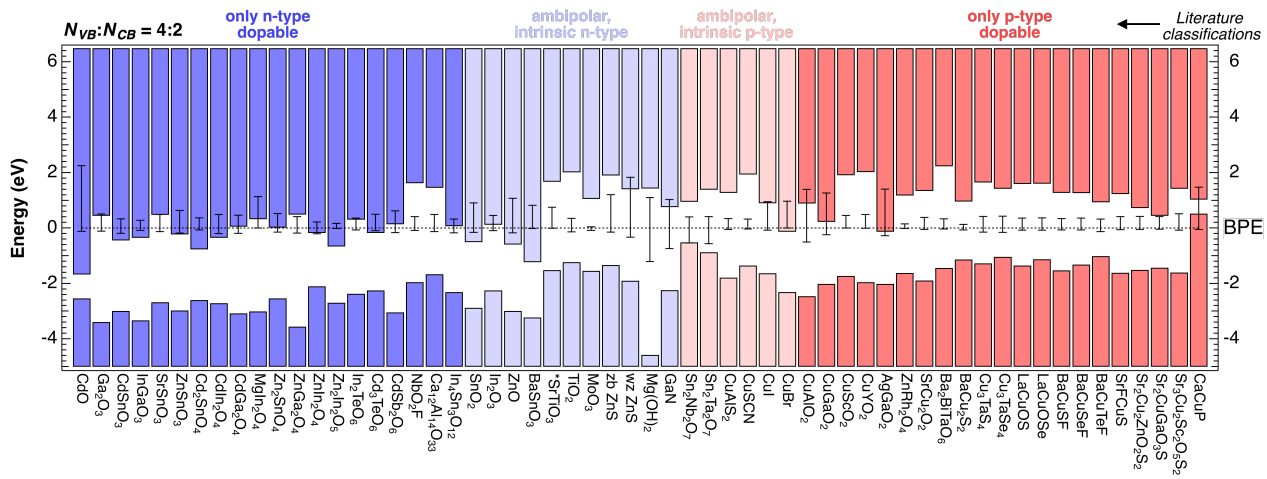

Figure 6: HSE06 band structure calculations aligned to branch point energy (BPE) levels (dotted line at 0 eV), as described in the text, for representative materials from the transparent conductor test set. Blue compounds are n-type TCs that have not been doped p-type, red are p-type TCs that have not been doped n-type, light blue are intrinsically n-type compounds that have also been doped p-type and studied as TCs, and light red are intrinsically p-type compounds that have also been doped n-type and studied as TCs. Calculations are performed with $N_{VB} = 4$ and $N_{CB} = 2$ (i.e. N_{VB}:N_{CB} = 4:2), following Schleife et al. (except for $SrTiO_3$, with an *, where we show N_{VB}:N_{CB} = 6:3 because of its triply degenerate VBM) and error bars indicate how computed BPE changes with different selection of N_{CB} and N_{VB} (and constant energy gap; c.f. SI).[107]

low achieved dopings,[99] while $Ca_{12}Al_{14}O_{33}$ is a unique cage-like structure with a completely localized (flat) VB that drags down then BPE.[111] In contrast, most of the p-type TCs in the test set have BPEs in the middle of the gap, and on average higher than mid-gap energy for N_{VB}:N_{CB} = 4:2. Even within error bars, only one p-type TC and two ambipolar p-type TCs (10% of the intrinsic p-type compounds) have a BPE in or below the lower quartile of the band gap, which would indicate favorable p-type doping. These mid-gap BPEs provide no evidence of favored n-type or p-type dopability, though they do not rule out the possibility for p-type doping (with the exception of $CuGaO_2$ and $AgGaO_2$, which would be expected n-type from BPE calculations; interestingly, we saw earlier that $CuGaO_2$ has an exceptionally low p-type dopability, and to our knowledge the carrier concentration of $AgGaO_2$ has not been reported). This disparity between BPE in n- and p-type TCs is possibly due to large dispersions in the CB and smaller dispersions in the VB, as well as larger spacing between individual bands in the CB, such that the average is skewed towards the CB.[107]

About half of the intrinsic n-type ambipolar semiconductors have BPEs near the CB,

while TiO_2, $SrTiO_3$, MoO_3, and both ZnS polymorphs do not. The intrinsic p-type ambipolar semiconductors CuI and CuBr exhibit BPEs near the CB within their respective error bars. We comment that some of these ambipolar semiconductors can be doped to far higher concentrations than others, and that some of these ambipolar doping cases have incurred controversy (e.g. p-doping of ZnO has been reported to be unstable and change to n-type after days or weeks).[112] Additionally, it is possible that some materials listed as n- or p-doped in Figure 6 could prove to be ambipolar under further experimental investigation, especially in p-type material systems that have not yet been extensively examined.

Figure 6 indicates that BPE may indeed be useful as a qualitative descriptor in high-throughput TC screenings, in particular to rule out materials that are very unlikely to be n- or p-type dopable. Furthermore, the analysis suggests that a p-type TC may be successfully identified by a mid-gap BPE. On the other hand, it is also feasible that the lack of an outstanding p-type TC is reflected by the lack of BPEs in or near the VB. Despite these correlations, this analysis is inherently biased in that it only includes materials from the test set; the calculation of a BPE near or within the CB does not indicate high n-type conductivity.

Additionally, BPE does not seem to indicate much about the degree to which a material can be doped or to which conditions favor a particular doping. In the SI we plot carrier concentration as a function of the position of the BPE referenced to the band gap, but see no significant correlation. We also compare BPE alignment to ionization potential alignment from the literature for a representative subset of TCs, observing only a minor correlation (c.f. SI). In particular for p-type materials, we have shown that in-depth defect calculations are required in order to more accurately assess dopability.[113] Calculation of extrinsic defects is necessary to select possible dopants; these have been performed for many of the state-of-the-art reported TCs.[114] To advance materials discovery applications, codes such at PyCDT and Pylada will facilitate high-throughput defect calculations that could be interfaced to computational materials science databases.[115,116]

Screening the test set

We now return to the question initially posed: are the descriptors within this screening procedure robust enough to predict experimentally realized TC candidates? Specifically, how many n-type and p-type TCs in the test set would successfully permeate the screening funnel in Figure 1? Recall that the test set includes both "good" transparent conductors and "ok" transparent conductors, so for this thought experiment we restrict the test set to "good" experimental TCs. These are materials with a maximum reported experimental optical gap ≥ 3.1 eV, corresponding approximately to transparency across the entire visible spectrum, and a somewhat arbitrarily chosen maximum reported conductivity ≥ 10 S/cm, corresponding to conductivities useful for solar cell transparent contacts. One can visualize this new set by placing a cutoff on the y-axes of both Figures 4 and 5. This reduces the set from 29 to 22 n-type TCs and from 45 to 12 p-type TCs (34 total).

As a sensitivity analysis, we first apply the following screening criteria to both n- and p-type TCs, representative of previously used cutoffs in the literature (c.f. bullet points in Introduction): $E_{hull} < 25$ meV/atom, PBE $E_g > 1$ eV, $m^* < 1$, maximum BPE $> 0.25E_g$ for n-type and minimum BPE $< 0.75E_g$ for p-type (i.e. including mid-gap state BPEs, with 0 eV referenced at the VBM and E_g at the CBM). We find that 7 of the 22 "good" n-type compounds emerge from this screening (most false negatives due to band gap cutoff, two from E_{hull}), and only 2 of the 12 "good" p-type compounds emerge (false negatives from E_{hull}, gap, and m^* cutoff). These criteria only pass 26% of compounds through the funnel.

Next, guided by the findings of Figures 3, 4, 5 and 6, we relax the limits to $E_{hull} < 100$ meV/atom, PBE $E_g > 0.5$ eV, $m_e^* < 1$, $m_h^* < 3$ (using planar m^* for layered and highly non-isotropic structures), maximum BPE $> 0.5E_g$ for n-type (to represent the asymmetry) and retain minimum BPE $< 0.75E_g$ for p-type. These criteria correctly pass 16 of the 22 "good" n-type and 11 of the 12 "good" p-type materials, accounting for approximately 80% of the set. Hence, a significantly improved number of true positives emerges from the funnel after adjusting the parameters using the insights gained from this study. The seven compounds

that did not pass are n-type CdO, $ZnIn_2O_4$, $BaSnO_3$, Cd_3TeO_6, Cd_2SnO_4, TiO_2 and p-type ZnO. The first five n-type false negatives were filtered out because of their low PBE band gaps, TiO_2 was filtered out due to its high m^*, and p-type ZnO was filtered out because of its BPE inside the conduction band (correctly reflecting the difficulty of doping ZnO p-type). In the SI we plot a sensitivity analysis for other choices of cutoffs for comparison. As an example of sensitivity, if the p-type minimum BPE is set to $< 0.5E_g$, only one of the "good" p-type compounds emerges. It also may be valuable to screen using direct gap; in our second example, setting direct PBE $E_g > 0.5$ eV would include $ZnIn_2O_4$ and $BaSnO_3$ and pass 85% of the set. However, we emphasize again that this analysis does not include the increase of false positives that would be included in a relaxation of screening cutoffs, and ultimately researchers must balance their tolerance for false positives and false negatives in order to decide an appropriate threshold.

Summary and conclusions

To motivate and strengthen the foundation upon which computational materials discovery efforts rely, we have computed a series of ground state derived descriptor properties for a test set of 74 state-of-the-art n-type and p-type transparent conductors (TCs), and compared them to their experimentally reported properties. First, we investigated stability of these compounds against decomposition by calculating their energies above the convex hull (E_{hull}) and a new viable descriptor: energy above the Pourbaix hull (E_{pb}). We found $E_{hull} < 100$ meV/atom to be an appropriate cutoff to represent thermodynamic stability for the test set TCs, and $E_{pb} < 1$ eV/atom to represent moisture stability. Second, investigation of the band gap showed that despite the conventional experimental optical gap requirement of 3.1 eV for TCs, a low PBE cutoff of approximately 0.5 eV is necessary to include most of the state-of-the-art TC materials in the test set. HSE06 gaps more closely approximate but still underestimate experimentally reported values, which can vary drastically depending

on dopant and processing conditions. On the other hand, we note that selecting a low PBE cutoff incurs similar selectivity as a mid-range HSE06 cutoff, which advocates the use of the least computationally expensive functional. Although this loosened criteria would allow in more false positives, we want to leave the possibility open for design of new p-type TCs with Burstein-Moss shifts and band engineering strategies, as in many of the test set materials. Third, by comparing computed effective mass and conductivity we found a much steeper and more correlated reciprocity in n-type materials than p-type, though high performing p-type TCs were shown to reach higher conductivities for a given effective mass. This suggests a lenient effective mass criteria of approximately $m_h^* \leq 3$ could be used in screenings. We speculate that a new transparent, low m_h^* material with minimal carrier compensation may, upon optimization, achieve p-type conductivities as high as the best n-type TCs, however we caution that this presumption relies on the limited number of p-type TCs in the test set. And fourth, branch point energy (BPE) calculations within a reasonable range of uncertainty predict most n-type TCs to have the propensity for n-type doping, while the mid-gap BPEs found in most p-type TCs rule out n-type doping but do not confirm p-type doping. This demonstrates that BPE may indeed be employed as a meaningful screening parameter, though defect calculations are still necessary to confirm p-type dopability. We reiterate that these four steps would just be the initial, broad steps in a high-throughput computational screening; more refinements should ultimately be incorporated subsequently, e.g. band alignment and defect studies.

We acknowledge some shortcomings of this study and the TC test set that we compiled. First, this test set only contains materials that have been confirmed to various degrees as promising research directions, rendering the study vulnerable to self-selection bias. This emphasizes the need for publication of more robust, experimental data, including also so-called "failed TCs" - e.g. negative data points. Similarly, the inclusion of a material in the set does not guarantee that it is a suitable transparent conductor (e.g. $CdSnO_3$ has been studied as a TC, but is not used commercially due to its low transparency).[117] Furthermore, the set is

still small in terms of determining trends with statistical significance. The number of studies does not necessarily correlate to nor indicate high performance (e.g. $CuAlO_2$ also has not been able to achieve optimal dopings and transparencies, even though it was considered the first p-type TC and has been heavily studied). Additionally, many of the test set materials are "doped" to very high concentrations (e.g. 20% Mg in $Mg_xLa_{1-x}CuOSe$)[118] or even form a mixed-phase composite (e.g. Cu_xS:ZnS) such that the electronic structure is significantly altered,[119] which will in turn deviate effective mass, band gap, and other electronic properties from those of the bulk material. Hence the analysis presented here may not be representative of properties achieved in practice. Finally, we emphasize that DFT is a ground state methodology, and in this study excited state effects (which are necessary for studying optoelectronic properties) are neglected, as well as temperature dependent scattering mechanisms. Overall, the bulk properties that we compute are not necessarily directly translatable into application performance, e.g. properties of thin film TCs, but here we have assessed the degree to which DFT properties can serve as a proxy to experimental TC properties.

Despite these shortcomings, this study justifies the use of an initial screening funnel using the simple DFT-based descriptors E_{hull}, E_g, m^*, and BPE, and provides estimates of cutoffs to employ in future screenings. The context provided on how experimentally achieved properties compare to analogous computed properties should be useful to both theorists and experimentalists working to develop new p-type transparent conductors. To enable further exploration of these relations and expansion upon the data set, we have made the TC test set publicly available in an interactive, query-able, and editable format through MPContribs, the Materials Project's Community Contribution Framework.[120,121] The investigation presented here has revealed the importance of assessing a screening funnel before applying it to a large database to discover new materials. We anticipate that this approach may be successfully applied to other fields in order to limit false positives and accelerate the discovery of new materials to enable crucial energy innovations.

Acknowledgements

This work was supported as part of the Center for Next Generation Materials by Design (CNGMD), an Energy Frontier Research Center funded by the U.S. Department of Energy, Office of Science, Basic Energy Sciences. R.W.R. was supported by the NSF Graduate Research Fellowship Program (GRFP) under Grant Numbers DGE1106400 and DGE1752814, and by the U.C. Berkeley Chancellor's Fellowship. D.B. was supported by the U.S. Department of Energy, Office of Science, Office of Basic Energy Sciences, Materials Sciences and Engineering Division under Contract No. DE-AC02-05-CH11231: Materials Project program KC23MP. A.J. and A.F. were funded by the U.S. Department of Energy, Office of Basic Energy Sciences, Early Career Research Program. This work used resources of the National Energy Research Scientific Computing Center (NERSC) at Lawrence Berkeley National Laboratory, supported by the BES of the U.S. DOE under Contract No. DE-AC02-05CH11231. The authors thank Dr. Joel Varley, Prof. Joel Ager, Prof. Geoffroy Hautier, Dr. Andriy Zakutayev, Dr. Joseph Montoya, Prof. Arunima Singh, Dr. Patrick Huck, Dr. Matthew Horton, Eric Sivonxay and John Dagdelen for insightful discussions and assistance.

Supporting information

The following are available free of charge.

- SI-TC-benchmark.pdf: Information on test set compilation, methodology considerations, gap analysis, plasma wavelength, transport considerations, BPE sensitivity analyses, literature comparisons of BPE and ionization potential, etc.
- SI-TC-benchmark-set.xlsx: A table of test set materials, their properties of interest discussed in this manuscript, and their corresponding references.

References

(1) Holdren, J. P. Materials genome initiative for global competitiveness. *National Science and technology council OSTP. Washington, USA* **2011**, 1–18.

(2) Jain, A.; Ong, S. P.; Hautier, G.; Chen, W.; Richards, W. D.; Dacek, S.; Cholia, S.; Gunter, D.; Skinner, D.; Ceder, G.; Persson, K. A. The Materials Project: A materials genome approach to accelerating materials innovation. *APL Materials* **2013**, *1*, 011002.

(3) Stevanović, V.; Lany, S.; Zhang, X.; Zunger, A. Correcting density functional theory for accurate predictions of compound enthalpies of formation: Fitted elemental-phase reference energies. *Phys. Rev. B* **2012**, *85*, 115104.

(4) Lany, S. Band-structure calculations for the 3*d* transition metal oxides in *GW*. *Phys. Rev. B* **2013**, *87*, 085112.

(5) Lany, S. Semiconducting transition metal oxides. *J. Phys.: Condens. Matter* **2015**, *27*, 283203.

(6) Saal, J. E.; Kirklin, S.; Aykol, M.; Meredig, B.; Wolverton, C. Materials design and discovery with high-throughput density functional theory: the open quantum materials database (OQMD). *Jom* **2013**, *65*, 1501–1509.

(7) Curtarolo, S.; Setyawan, W.; Wang, S.; Xue, J.; Yang, K.; Taylor, R. H.; Nelson, L. J.; Hart, G. L.; Sanvito, S.; Buongiorno-Nardelli, M.; Mingo, N. AFLOWLIB. ORG: A distributed materials properties repository from high-throughput ab initio calculations. *Comput. Mater. Sci.* **2012**, *58*, 227–235.

(8) Kirklin, S.; Meredig, B.; Wolverton, C. High-Throughput Computational Screening of New Li-Ion Battery Anode Materials. *Adv. Energy Mater.* **2013**, *3*, 252–262.

(9) Korth, M. Large-scale virtual high-throughput screening for the identification of new battery electrolyte solvents: evaluation of electronic structure theory methods. *Phys. Chem. Chem. Phys.* **2014**, *16*, 7919–7926.

(10) Castelli, I. E.; Olsen, T.; Datta, S.; Landis, D. D.; Dahl, S.; Thygesen, K. S.; Jacobsen, K. W. Computational screening of perovskite metal oxides for optimal solar light capture. *Energy Environ. Sci.* **2012**, *5*, 5814–5819.

(11) Wu, X.; Coutts, T. J.; Mulligan, W. P. Properties of transparent conducting oxides formed from CdO and ZnO alloyed with SnO2 and In2O3. *J. Vac. Sci. Technol., A* **1997**, *15*, 1057–1062.

(12) Kuhar, K.; Crovetto, A.; Pandey, M.; Thygesen, K. S.; Seger, B.; Vesborg, P. C. K.; Hansen, O.; Chorkendorff, I.; Jacobsen, K. W. Sulfide perovskites for solar energy conversion applications: computational screening and synthesis of the selected compound LaYS3. *Energy Environ. Sci.* **2017**, *10*, 2579–2593.

(13) Kuhar, K.; Pandey, M.; Thygesen, K. S.; Jacobsen, K. W. High-Throughput Computational Assessment of Previously Synthesized Semiconductors for Photovoltaic and Photoelectrochemical Devices. *ACS Energy Lett.* **2018**, *3*, 436–446.

(14) Hachmann, J.; Olivares-Amaya, R.; Jinich, A.; Appleton, A. L.; Blood-Forsythe, M. A.; Seress, L. R.; Roman-Salgado, C.; Trepte, K.; Atahan-Evrenk, S.; Er, S. Lead candidates for high-performance organic photovoltaics from high-throughput quantum chemistry-the Harvard Clean Energy Project. *Energy Environ. Sci.* **2014**, *7*, 698–704.

(15) Jain, A.; Shin, Y.; Persson, K. A. Computational predictions of energy materials using density functional theory. *Nat. Rev. Mater.* **2016**, *1*, 15004.

(16) Green, M. L.; Choi, C.; Hattrick-Simpers, J.; Joshi, A.; Takeuchi, I.; Barron, S.; Campo, E.; Chiang, T.; Empedocles, S.; Gregoire, J.; Kusne, A. Fulfilling the promise of the materials genome initiative with high-throughput experimental methodologies. *Appl. Phys. Rev.* **2017**, *4*, 011105.

(17) Zunger, A. Inverse design in search of materials with target functionalities. *Nat. Rev. Chem.* **2018**, *2*, 0121.

(18) Ohta, H.; Orita, M.; Hirano, M.; Tanji, H.; Kawazoe, H.; Hosono, H. Highly electrically conductive indium–tin–oxide thin films epitaxially grown on yttria-stabilized zirconia (100) by pulsed-laser deposition. *Appl. Phys. Lett.* **2000**, *76*, 2740–2742.

(19) Rauf, I. A. Structure and properties of tin-doped indium oxide thin films prepared by reactive electron-beam evaporation with a zone-confining arrangement. *J. Appl. Phys.* **1996**, *79*, 4057–4065.

(20) Bhachu, D. S.; Waugh, M. R.; Zeissler, K.; Branford, W. R.; Parkin, I. P. Textured Fluorine-Doped Tin Dioxide Films formed by Chemical Vapour Deposition. *Chem. Eur. J* **2011**, *17*, 11613–11621.

(21) Agashe, C.; Hüpkes, J.; Schöpe, G.; Berginski, M. Physical properties of highly oriented spray-deposited fluorine-doped tin dioxide films as transparent conductor. *Sol. Energy Mater. Sol. Cells* **2009**, *93*, 1256–1262.

(22) Izaki, M.; Omi, T. Transparent zinc oxide films prepared by electrochemical reaction. *Appl. Phys. Lett.* **1996**, *68*, 2439–2440.

(23) Agura, H.; Suzuki, A.; Matsushita, T.; Aoki, T.; Okuda, M. Low resistivity transparent conducting Al-doped ZnO films prepared by pulsed laser deposition. *Thin Solid Films* **2003**, *445*, 263–267.

(24) Morales-Masis, M.; De Wolf, S.; Woods-Robinson, R.; Ager, J. W.; Ballif, C. Transparent electrodes for efficient optoelectronics. *Adv. Electron. Mater.* **2017**, *3*, 1600529.

(25) Banerjee, A.; Ghosh, C. K.; Chattopadhyay, K. Effect of excess oxygen on the electrical properties of transparent p-type conducting CuAlO thin films. *Sol. Energy Mater. Sol. Cells* **2005**, *89*, 75–83.

(26) Delahoy, A. E.; Guo, S. Y. Transparent and semitransparent conducting film deposition by reactive-environment, hollow cathode sputtering. *J. Vac. Sci. Technol., A* **2005**, *23*, 1215–1220.

(27) Kawazoe, H.; Yasukawa, M.; Hyodo, H. P-type electrical conduction in transparent thin films of CuAlO2. *Nature* **1997**, *289*, 939–942.

(28) Yanagi, H.; ichiro Inoue, S.; Ueda, K.; Kawazoe, H.; Hosono, H.; Hamada, N. Electronic structure and optoelectronic properties of transparent p-type conducting CuAlO2. *J. Appl. Phys.* **2000**, *88*, 4159.

(29) Snure, M.; Tiwari, A. CuBO2: A p-type transparent oxide. *Appl. Phys. Lett.* **2007**, *91*, 092123.

(30) Ruttanapun, C. Optical and electronic properties of delafossite CuBO2 p-type transparent conducting oxide. *J. Appl. Phys.* **2013**, *114*, 113108.

(31) Nagarajan, R.; Draeseke, A. D.; Sleight, A. W.; Tate, J. p-type conductivity in CuCr1-xMgxO2 films and powders. *J. Appl. Phys.* **2001**, *89*, 8022–8025.

(32) Farrell, L.; Norton, E.; Smith, C. M.; Caffrey, D.; Shvets, I. V.; Fleischer, K. Synthesis of nanocrystalline Cu deficient CuCrO 2-a high figure of merit p-type transparent semiconductor. *J. Mater. Chem. C* **2016**, *4*, 126–134.

(33) Mandal, P.; Mazumder, N.; Saha, S.; Ghorai, U. K.; Roy, R.; Das, G. C.; Chattopadhyay, K. K. A scheme of simultaneous cationic–anionic substitution in CuCrO2for transparent and superiorp-type transport. *J. Phys. D: Appl. Phys.* **2016**, *49*, 275109.

(34) Ruttanapun, C.; Prachamon, W.; Wichainchai, A. Optoelectronic properties of Cu1xPtxFeO2 (0 x 0.05) delafossite for p-type transparent conducting oxide. *Curr. Appl. Phys.* **2012**, *12*, 166–170.

(35) Read, C. G.; Park, Y.; Choi, K.-S. Electrochemical Synthesis of p-Type CuFeO2 Electrodes for Use in a Photoelectrochemical Cell. *J. Phys. Chem. Lett.* **2012**, *3*, 1872–1876.

(36) Han, M.; Jiang, K.; Zhang, J.; Yu, W.; Li, Y.; Hu, Z.; Chu, J. Structural, electronic band transition and optoelectronic properties of delafossite CuGa 1- x Cr x O 2 (0 x 1) solid solution films grown by the sol-gel method. *J. Mater. Chem.* **2012**, *22*, 18463–18470.

(37) Duan, N.; Sleight, A. W.; Jayaraj, M. K.; Tate, J. Transparent p-type conducting CuScO2x films. *Appl. Phys. Lett.* **2000**, *77*, 1325–1326.

(38) Yanagi, H.; Park, S.; Draeseke, A.; Keszler, D.; Tate, J. P-type conductivity in transparent oxides and sulfide fluorides. *J. Solid State Chem.* **2003**, *175*, 34–38.

(39) Jayaraj, M.; Draeseke, A.; Tate, J.; Sleight, A. p-Type transparent thin films of CuY1-xCaxO2. *Thin Solid Films* **2001**, *397*, 244–248.

(40) Zakutayev, A.; Paudel, T. R.; Ndione, P. F.; Perkins, J. D.; Lany, S.; Zunger, A.; Ginley, D. S. Cation off-stoichiometry leads to high p-type conductivity and enhanced transparency in Co 2 ZnO 4 and Co 2 NiO 4 thin films. *Phys. Rev. B* **2012**, *85*, 085204.

(41) Dekkers, M.; Rijnders, G.; Blank, D. H. Zn Ir 2 O 4, ap-type transparent oxide semiconductor in the class of spinel zinc-d 6-transition metal oxide. *Appl. Phys. Lett.* **2007**, *90*, 021903.

(42) Ueda, K.; Inoue, S.; Hirose, S.; Kawazoe, H.; Hosono, H. Transparent p-type semiconductor: LaCuOS layered oxysulfide. *Appl. Phys. Lett.* **2000**, *77*, 2701–2703.

(43) Hiramatsu, H.; Ueda, K.; Ohta, H.; Hirano, M.; Kamiya, T.; Hosono, H. Degenerate p-type conductivity in wide-gap LaCuOS1-xSex (x=0–1) epitaxial films. *Appl. Phys. Lett.* **2003**, *82*, 1048–1050.

(44) Hautier, G.; Miglio, A.; Ceder, G.; Rignanese, G.-M.; Gonze, X. Identification and design principles of low hole effective mass p-type transparent conducting oxides. *Nat. Commun.* **2013**, *4*, 2292.

(45) Bhatia, A.; Hautier, G.; Nilgianskul, T.; Miglio, A.; Sun, J.; Kim, H. J.; Kim, K. H.; Chen, S.; Rignanese, G.-M.; Gonze, X.; Suntivich, J. High-mobility bismuth-based transparent p-type oxide from high-throughput material screening. *Chem. Mater.* **2015**, *28*, 30–34.

(46) Varley, J. B.; Miglio, A.; Ha, V. A.; Van Setten, M. J.; Rignanese, G. M.; Hautier, G. High-Throughput Design of Non-oxide p-Type Transparent Conducting Materials: Data Mining, Search Strategy, and Identification of Boron Phosphide. *Chem. Mater.* **2017**, *29*, 2568–2573.

(47) Sarmadian, N.; Saniz, R.; Partoens, B.; Lamoen, D. Easily doped p-type, low hole effective mass, transparent oxides. *Sci. Rep.* **2016**, *6*, 1–9.

(48) Williamson, B. A. D.; Buckeridge, J.; Brown, J.; Ansbro, S.; Palgrave, R. G.; Scanlon, D. O. Engineering Valence Band Dispersion for High Mobility p-Type Semiconductors. *Chem. Mater.* **2016**, *29*, 2402–2413.

(49) Shi, J.; Cerqueira, T. F.; Cui, W.; Nogueira, F.; Botti, S.; Marques, M. A. High-throughput search of ternary chalcogenides for p-type transparent electrodes. *Sci. Rep.* **2017**, *7*, 1–13.

(50) Aykol, M.; Dwaraknath, S. S.; Sun, W.; Persson, K. A. Thermodynamic limit for synthesis of metastable inorganic materials. *Sci. Adv.* **2018**, *4*, eaaq0148.

(51) Sun, W.; Dacek, S. T.; Ong, S. P.; Hautier, G.; Jain, A.; Richards, W. D.; Gamst, A. C.; Persson, K. A.; Ceder, G. The thermodynamic scale of inorganic crystalline metastability. *Sci. Adv.* **2016**, *2*, e1600225.

(52) Singh, A. K.; Zhou, L.; Shinde, A.; Suram, S. K.; Montoya, J. H.; Winston, D.; Gregoire, J. M.; Persson, K. A. Electrochemical Stability of Metastable Materials. *Chem. Mater.* **2017**, *29*, 10159–10167.

(53) Ricci, F.; Chen, W.; Aydemir, U.; Snyder, G. J.; Rignanese, G.-M.; Jain, A.; Hautier, G. An ab initio electronic transport database for inorganic materials. *Sci. Data* **2017**, *4*, 170085.

(54) Kormath Madam Raghupathy, R.; Kühne, T. D.; Felser, C.; Mirhosseini, H. Rational design of transparent p-type conducting non-oxide materials from high-throughput calculations. *J. Mater. Chem. C* **2018**, *6*, 541–549.

(55) Hautier, G.; Ong, S. P.; Jain, A.; Moore, C. J.; Ceder, G. Accuracy of density functional theory in predicting formation energies of ternary oxides from binary oxides and its implication on phase stability. *Phys. Rev. B: Condens. Matter Mater. Phys.* **2012**, *85*, 155208.

(56) Adachi, C.; Nagai, K.; Tamoto, N. Molecular design of hole transport materials for obtaining high durability in organic electroluminescent diodes. *Appl. Phys. Lett.* **1995**, *66*, 2679–2681.

(57) van de Groep, J.; Spinelli, P.; Polman, A. Transparent conducting silver nanowire networks. *Nano Lett.* **2012**, *12*, 3138–44.

(58) Zhang, X.; Zhang, L.; Perkins, J. D.; Zunger, A. Intrinsic transparent conductors without doping. *Phys. Rev. Letters* **2015**, *115*, 176602.

(59) Ito, N.; Sato, Y.; Song, P.; Kaijio, A.; Inoue, K.; Shigesato, Y. Electrical and optical properties of amorphous indium zinc oxide films. *Thin solid films* **2006**, *496*, 99–103.

(60) Hautier, G.; Fischer, C.; Ehrlacher, V.; Jain, A.; Ceder, G. Data mined ionic substitutions for the discovery of new compounds. *Inorg. Chem.* **2010**, *50*, 656–663.

(61) Blöchl, P. E. Projector augmented-wave method. *Phys. Rev. B* **1994**, *50*, 17953.

(62) Kresse, G.; Joubert, D. From ultrasoft pseudopotentials to the projector augmented-wave method. *Phys. Rev. B* **1999**, *59*, 1758–1775.

(63) Kresse, G.; Hafner, J. Ab initio molecular dynamics for liquid metals. *Phys. Rev. B* **1993**, *47*, 558–561.

(64) Kresse, G.; Furthmüller, J. Efficient iterative schemes for ab initio total-energy calculations using a plane-wave basis set. *Phys. Rev. B* **1996**, *54*, 11169.

(65) Perdew, J. P.; Burke, K.; Ernzerhof, M. Generalized gradient approximation made simple. *Phys. Rev. Letters* **1996**, *77*, 3865.

(66) Mathew, K. et al. Atomate: A high-level interface to generate, execute, and analyze computational materials science workflows. *Comput. Mater. Sci.* **2017**, *139*, 140–152.

(67) Wang, Y.; Liu, M.; Huang, F.; Chen, L.; Li, H.; Lin, X.; Wang, W.; Xia, Y. Solution-Processed p-Type Transparent Conducting BaCu2S2Thin Film. *Chem. Mater.* **2007**, *19*, 3102–3104.

(68) Ong, S. P.; Richards, W. D.; Jain, A.; Hautier, G.; Kocher, M.; Cholia, S.; Gunter, D.; Chevrier, V. L.; Persson, K. A.; Ceder, G. Python Materials Genomics (pymatgen): A robust, open-source python library for materials analysis. *Comput. Mater. Sci.* **2013**, *68*, 314 – 319.

(69) Persson, K. A.; Waldwick, B.; Lazic, P.; Ceder, G. Prediction of solid-aqueous equilibria: Scheme to combine first-principles calculations of solids with experimental aqueous states. *Phys. Rev. B* **2012**, *85*, 235438.

(70) Heyd, J.; Scuseria, G. E.; Ernzerhof, M. Hybrid functionals based on a screened Coulomb potential. *J. Chem. Phys.* **2003**, *118*, 8207–8215.

(71) Madsen, G. K. H.; Singh, D. J. BoltzTraP. A code for calculating band-structure dependent quantities. *Comput. Phys. Commun.* **2006**, *175*, 67–71.

(72) Stanton, C. J.; Wilkins, J. W. Nonequilibrium current fluctuations in semiconductors: A Boltzmann-equation-Green-function approach. *Phys. Rev. B* **1987**, *35*, 9722–9734.

(73) Hayashi, T.; Deura, M.; Ohkawa, K. High stability and efficiency of GaN photocatalyst for hydrogen generation from water. *Jpn. J. Appl. Phys.* **2012**, *51*, 112601.

(74) Moriga, T.; Ishida, K.; Yamamoto, K.; Yoshinari, A.; Murai, K.-I. Structural analysis of homologous series of Zn k In2O k+ 3 (k= 3, 5, 7) and Zn k InGaO k+ 3 (k= 1, 3, 5) as thermoelectric materials. *Mater. Res. Innovations* **2009**, *13*, 348–351.

(75) Nakamura, M.; Kimizuka, N.; Mohri, T. The phase relations in the In2O3 Fe2ZnO4 ZnO system at 1350 C. *J. Solid State Chem.* **1990**, *86*, 16–40.

(76) Minami, T.; Miyata, T.; Yamamoto, T. Stability of transparent conducting oxide films for use at high temperatures. *J. Vac. Sci. Technol., A* **1999**, *17*, 1822–1826.

(77) Sun, W.; Bartel, C.; Arca, E.; Bauers, S.; Matthews, B.; Orvananos, B.; Chen, B.-R.; Toney, M. F.; Schelhas, L. T.; Tumas, W.; Tate, J.; Zakutayev, A.; Lany, S.; Holder, A.; Ceder, G. A Map of the Inorganic Ternary Metal Nitrides. *arXiv preprint arXiv:1809.09202* **2018**,

(78) Arca, E.; Lany, S.; Perkins, J. D.; Bartel, C. J.; Mangum, J.; Sun, W.; Holder, A.; Ceder, G.; Gorman, B.; Teeter, G.; Tumas, B.; Zakutayev, A. Redox-Mediated Stabilization in Zinc Molybdenum Nitrides. *J. Am. Chem. Soc.* **2018**, *140*, 4293–4301.

(79) Pankove, J. I. *Optical processes in semiconductors*; Courier Corporation, 1975.

(80) Tauc, J.; Grigorovici, R.; Vancu, A. Optical properties and electronic structure of amorphous germanium. *Phys. Status Solidi B* **1966**, *15*, 627–637.

(81) Morales, A. E.; Mora, E. S.; Pal, U. Use of diffuse reflectance spectroscopy for optical characterization of un-supported nanostructures. *Rev. Mex. Fis.* **2007**, *53*, 18–22.

(82) Heyd, J.; Scuseria, G. E. Efficient hybrid density functional calculations in solids: Assessment of the Heyd-Scuseria-Ernzerhof screened Coulomb hybrid functional. *J. Chem. Phys.* **2004**, *121*, 1187–1192.

(83) Chan, M.; Ceder, G. Efficient band gap prediction for solids. *Phys. Rev. Letters* **2010**, *105*, 196403.

(84) Yan, Q.; Yu, J.; Suram, S. K.; Zhou, L.; Shinde, A.; Newhouse, P. F.; Chen, W.; Li, G.; Persson, K. A.; Gregoire, J. M.; Neaton, J. B. Solar fuels photoanode materials discovery by integrating high-throughput theory and experiment. *Proc. Natl. Acad. Sci. U.S.A.* **2017**, *114*, 3040–3043.

(85) Fleischer, K.; Norton, E.; Mullarkey, D.; Caffrey, D.; Shvets, I. V. Quantifying the Performance of P-Type Transparent Conducting Oxides by Experimental Methods. *Materials* **2017**, *10*, 1019.

(86) Coulter, J. B.; Birnie III, D. P. Assessing Tauc plot slope quantification: ZnO thin films as a model system. *Phys. Status Solidi B* **2018**, *255*, 1700393.

(87) Dressel, M.; Grüner, G. Electrodynamics of solids: optical properties of electrons in matter. 2002.

(88) Moss, T. The interpretation of the properties of indium antimonide. *Proc. Phys. Soc., London, Sect. B* **1954**, *67*, 775–782.

(89) Burstein, E. Anomalous optical absorption limit in InSb. *Phys. Rev.* **1954**, *93*, 632–633.

(90) Klein, A.; Körber, C.; Wachau, A.; Säuberlich, F.; Gassenbauer, Y.; Harvey, S. P.; Proffit, D. E.; Mason, T. O. Transparent conducting oxides for photovoltaics: Manipulation of fermi level, work function and energy band alignment. *Materials* **2010**, *3*, 4892–4914.

(91) Granerød, C. S.; Bilden, S. R.; Aarholt, T.; Yao, Y.-F.; Yang, C.; Look, D. C.; Vines, L.; Johansen, K. M.; Prytz, Ø. Direct observation of conduction band plasmons and the related Burstein-Moss shift in highly doped semiconductors: A STEM-EELS study of Ga-doped ZnO. *Phys. Rev. B* **2018**, *98*, 115301.

(92) Fan, H. Infra-red absorption in semiconductors. *Rep. Prog. Phys.* **1956**, *19*, 107–155.

(93) Tsai, C.-Y.; Tsai, C.-Y.; Chen, C.-H.; Sung, T.-L.; Wu, T.-Y.; Shih, F.-P. Theoretical model for intravalley and intervalley free-carrier absorption in semiconductor lasers: Beyond the classical Drude model. *IEEE J. Quantum Electron.* **1998**, *34*, 552–559.

(94) Ueda, K.; Inoue, S.; Hosono, H.; Sarukura, N.; Hirano, M. Room-temperature excitons in wide-gap layered-oxysulfide semiconductor: LaCuOS. *Appl. Phys. Lett.* **2001**, *78*, 2333–2335.

(95) Van der Pauw, L. Determination of resistivity tensor and Hall tensor of anisotropic shape. *Philips Research Reports* **1961**, *16*, 187–195.

(96) Werner, F. Hall measurements on low-mobility thin films. *J. Appl. Phys.* **2017**, *122*, 135306.

(97) Hosono, H.; Paine, D. C. *Handbook of transparent conductors*; Springer Science & Business Media, 2010.

(98) Hitosugi, T.; Kamisaka, H.; Yamashita, K.; Nogawa, H.; Furubayashi, Y.; Nakao, S.; Yamada, N.; Chikamatsu, A.; Kumigashira, H.; Oshima, M.; Hirose, Y. Electronic band structure of transparent conductor: Nb-doped anatase TiO2. *Appl. Phys. Express* **2008**, *1*, 111203.

(99) Mizoguchi, H.; Orita, M.; Hirano, M.; Fujitsu, S.; Takeuchi, T.; Hosono, H. NbO2F: An oxyfluoride phase with wide band gap and electrochromic properties. *Appl. Phys. Lett.* **2002**, *80*, 4732–4734.

(100) Park, S.-M.; Ikegami, T.; Ebihara, K. Effects of substrate temperature on the properties of Ga-doped ZnO by pulsed laser deposition. *Thin Solid Films* **2006**, *513*, 90–94.

(101) Ellmer, K. Resistivity of polycrystalline zinc oxide films: current status and physical limit. *J. Phys. D: Appl. Phys.* **2001**, *34*, 3097–3108.

(102) Zhang, D.; Ma, H. Scattering mechanisms of charge carriers in transparent conducting oxide films. *Appl. Phys. A* **1996**, *62*, 487–492.

(103) Peng, H.; Zakutayev, A.; Lany, S.; Paudel, T. R.; dAvezac, M.; Ndione, P. F.; Perkins, J. D.; Ginley, D. S.; Nagaraja, A. R.; Perry, N. H.; Mason, T. O.; Zunger, A. Li-Doped Cr2MnO4: A New p-Type Transparent Conducting Oxide by Computational Materials Design. *Adv. Funct. Mater.* **2013**, *23*, 5267–5276.

(104) Yang, C.; Knei, M.; Lorenz, M.; Grundmann, M. Room-temperature synthesized copper iodide thin film as degenerate p-type transparent conductor with a boosted figure of merit. *Proc. Natl. Acad. Sci. U.S.A.* **2016**, *113*, 12929–12933.

(105) Varley, J.; Janotti, A.; Franchini, C.; Van de Walle, C. G. Role of self-trapping in luminescence and p-type conductivity of wide-band-gap oxides. *Phys. Rev. B* **2012**, *85*, 081109.

(106) Zunger, A. Practical doping principles. *Appl. Phys. Lett.* **2003**, *83*, 57–59.

(107) Schleife, A.; Fuchs, F.; Rödl, C.; Furthmüller, J.; Bechstedt, F. Branch-point energies and band discontinuities of III-nitrides and III-/II-oxides from quasiparticle band-structure calculations. *Appl. Phys. Lett.* **2009**, *94*, 012104.

(108) Varley, J. B.; Samanta, A.; Lordi, V. Descriptor-Based Approach for the Prediction of Cation Vacancy Formation Energies and Transition Levels. *J. Phys. Chem. Lett.* **2017**, *8*, 5059–5063.

(109) Choi, M.; Posadas, A. B.; Rodriguez, C. A.; OHara, A.; Seinige, H.; Kellock, A. J.; Frank, M. M.; Tsoi, M.; Zollner, S.; Narayanan, V.; Demkov, A. A. Structural, optical, and electrical properties of strained La-doped SrTiO3 films. *J. Appl. Phys.* **2014**, *116*, 043705.

(110) Huang, W.; Nechache, R.; Li, S.; Chaker, M.; Rosei, F. Electrical and Optical Properties of Transparent Conducting p-Type SrTiO3 Thin Films. *J. Am. Ceram. Soc.* **2015**, *99*, 226–233.

(111) Kim, S. W.; Matsuishi, S.; Nomura, T.; Kubota, Y.; Takata, M.; Hayashi, K.; Kamiya, T.; Hirano, M.; Hosono, H. Metallic State in a Lime-Alumina Compound with Nanoporous Structure. *Nano Lett.* **2007**, *7*, 1138–1143.

(112) Park, C.; Zhang, S.; Wei, S.-H. Origin of p-type doping difficulty in ZnO: The impurity perspective. *Phys. Rev. B* **2002**, *66*, 073202.

(113) Lany, S.; Zunger, A. Assessment of correction methods for the band-gap problem and for finite-size effects in supercell defect calculations: Case studies for ZnO and GaAs. *Phys. Rev. B* **2008**, *78*, 235104.

(114) Lany, S.; Zunger, A. Dopability, intrinsic conductivity, and nonstoichiometry of transparent conducting oxides. *Phys. Rev. Letters* **2007**, *98*, 045501.

(115) Broberg, D.; Medasani, B.; Zimmermann, N. E.; Yu, G.; Canning, A.; Haranczyk, M.; Asta, M.; Hautier, G. PyCDT: A Python toolkit for modeling point defects in semiconductors and insulators. *Comput. Phys. Commun.* **2018**, *226*, 165 – 179.

(116) Goyal, A.; Gorai, P.; Peng, H.; Lany, S.; Stevanović, V. A computational framework for automation of point defect calculations. *Comput. Mater. Sci.* **2017**, *130*, 1–9.

(117) Shannon, R.; Gillson, J.; Bouchard, R. Single crystal synthesis and electrical properties of CdSnO3, Cd2SnO4, In2TeO6 and Cdln2O4. *J. Phys.: Condens. Matter* **1977**, *38*, 877–881.

(118) Hiramatsu, H.; Ueda, K.; Ohta, H.; Hirano, M.; Kamiya, T.; Hosono, H. Degenerate p-type conductivity in wide-gap LaCuOS1xSex (x=0-1) epitaxial films. *Appl. Phys. Lett.* **2003**, *82*, 1048–1050.

(119) Xu, X.; Bullock, J.; Schelhas, L. T.; Stutz, E. Z.; Fonseca, J. J.; Hettick, M.; Pool, V. L.; Tai, K. F.; Toney, M. F.; Fang, X.; Javey, A.; Wong, L. H.; Ager, J. W. Chemical Bath Deposition of p-Type Transparent, Highly Conducting (CuS)x:(ZnS)1–x Nanocomposite Thin Films and Fabrication of Si Heterojunction Solar Cells. *Nano Lett.* **2016**, *16*, 1925–1932.

(120) Huck, P.; Gunter, D.; Cholia, S.; Winston, D.; N'Diaye, A.; Persson, K. User applications driven by the community contribution framework MPContribs in the Materials Project. *Concurr Comput.* **2016**, *28*, 1982–1993.

(121) Woods-Robinson, R.; Huck, P. Transparent Conductors. `https://materialsproject.org/mpcontribs/transparent_conductors`, accessed October 28, 2018.

Graphical TOC Entry